

Development of a monochromatic crystal backlight imager for the recent double-cone ignition experiments

Chenglong Zhang(张成龙), Yihang Zhang(张翌航), Xiaohui Yuan(远晓辉), Zhe Zhang(张喆), Miaohua Xu(徐妙华), Yu Dai(戴羽), Yufeng Dong(董玉峰), Haochen Gu(谷昊琛), Zhengdong Liu(刘正东), Xu Zhao(赵旭), Yutong Li(李玉同), Yingjun Li(李英骏), Jianqiang Zhu(朱健强), and Jie Zhang(张杰)
Citation: Chin. Phys. B, 2024, 33 (**2**): 025201. DOI: 10.1088/1674-1056/ad1091
Journal homepage: http://cpb.iphy.ac.cn; http://iopscience.iop.org/cpb

What follows is a list of articles you may be interested in

Speeding-up direct implicit particle-in-cell simulations in bounded plasma by obtaining future electric field through explicitly propulsion of particles

Haiyun Tan(谭海云), Tianyuan Huang(黄天源), Peiyu Ji(季佩宇), Mingjie Zhou(周铭杰), Lanjian Zhuge(诸葛兰剑), and Xuemei Wu(吴雪梅)
Chin. Phys. B, 2023, 32 (**12**): 125204. DOI: 10.1088/1674-1056/acf449

Analytical model for Rayleigh—Taylor instability in conical target conduction region

Zhong-Yuan Zhu(朱仲源), Yun-Xing Liu(刘云星), Ying-Jun Li(李英骏), and Jie Zhang(张杰)
Chin. Phys. B, 2022, 31 (**10**): 105202. DOI: 10.1088/1674-1056/ac8731

Measurement of molybdenum ion density for L-mode and H-mode plasma discharges in the EAST tokamak

Yongcai Shen(沈永才), Hongming Zhang(张洪明), Bo Lyu(吕波), Yingying Li(李颖颖), Jia Fu(符佳), Fudi Wang(王福地), Qing Zang(臧庆), Baonian Wan(万宝年), Pan Pan(潘盼), Minyou Ye(叶民友)
Chin. Phys. B, 2020, 29 (**6**): 065206. DOI: 10.1088/1674-1056/ab8456

Areal density and spatial resolution of high energy electron radiography

Jiahao Xiao(肖家浩), Zimin Zhang(张子民), Shuchun Cao(曹树春), Ping Yuan(袁平), Xiaokang Shen(申晓康), Rui Cheng(程锐), Quantang Zhao(赵全堂), Yang Zong(宗阳), Ming Liu(刘铭), Xianming Zhou(周贤明), Zhongping Li(李中平), Yongtao Zhao(赵永涛), Chuanxiang Tang(唐传祥), Wenhui Huang(黄文会), Yingchao Du(杜应超), Wei Gai(盖炜)
Chin. Phys. B, 2018, 27 (**3**): 035202. DOI: 10.1088/1674-1056/27/3/035202

Influence of tip geometry on the spatial resolution of tip enhanced Raman mapping

Chao Zhang(张超), Bao-Qin Chen(陈宝琴), Zhi-Yuan Li(李志远)
Chin. Phys. B, 2016, 25 (**9**): 095203. DOI: 10.1088/1674-1056/25/9/095203

INSTRUMENTATION AND MEASUREMENT

Development of a monochromatic crystal backlight imager for the recent double-cone ignition experiments

Chenglong Zhang(张成龙)[1,2], Yihang Zhang(张翌航)[2], Xiaohui Yuan(远晓辉)[3,4], Zhe Zhang(张喆)[2,4,5,†], Miaohua Xu(徐妙华)[6,‡], Yu Dai(戴羽)[2,7], Yufeng Dong(董玉峰)[2,7], Haochen Gu(谷昊琛)[2,7], Zhengdong Liu(刘正东)[8,9], Xu Zhao(赵旭)[3,4], Yutong Li(李玉同)[2,4,5], Yingjun Li(李英骏)[1,§], Jianqiang Zhu(朱健强)[10], and Jie Zhang(张杰)[2,3,4]

[1] *State Key Laboratory for Geomechanics and Deep Underground Engineering, China University of Mining and Technology, Beijing* 100083, *China*
[2] *Beijing National Laboratory for Condensed Matter Physics, Institute of Physics, Chinese Academy of Sciences, Beijing* 100190, *China*
[3] *Key Laboratory for Laser Plasmas (MoE) and School of Physics and Astronomy, Shanghai Jiao Tong University, Shanghai* 200240, *China*
[4] *Collaborative Innovation Center of IFSA (CICIFSA), Shanghai Jiao Tong University, Shanghai* 200240, *China*
[5] *Songshan Lake Materials Laboratory, Dongguan* 523808, *China*
[6] *School of Science, China University of Mining and Technology (Beijing), Beijing* 100089, *China*
[7] *School of Physical Sciences, University of Chinese Academy of Sciences, Beijing* 100049, *China*
[8] *Department of Astronomy, Beijing Normal University, Beijing* 100875, *China*
[9] *Institute for Frontiers in Astronomy and Astrophysics, Beijing Normal University, Beijing* 102206, *China*
[10] *Key Laboratory of High Power Laser and Physics, Chinese Academy of Sciences, Shanghai* 201800, *China*

(Received 5 September 2023; revised manuscript received 1 November 2023; accepted manuscript online 29 November 2023)

We developed a monochromatic crystal backlight imaging system for the double-cone ignition (DCI) scheme, employing a spherically bent quartz crystal. This system was used to measure the spatial distribution and temporal evolution of the head-on colliding plasma from the two compressing cones in the DCI experiments. The influence of laser parameters on the x-ray backlighter intensity and spatial resolution of the imaging system was investigated. The imaging system had a spatial resolution of 10 μm when employing a CCD detector. Experiments demonstrated that the system can obtain time-resolved radiographic images with high quality, enabling the precise measurement of the shape, size, and density distribution of the plasma.

Keywords: double-cone ignition (DCI), spatial resolution, x-ray radiography

PACS: 52.57.–z, 52.57.Kk **DOI:** 10.1088/1674-1056/ad1091

1. Introduction

The double-cone ignition (DCI) is a new ignition scheme for inertial confinement fusion proposed by Zhang *et al.*,[1] in which two open–end head-on gold cones filled with segmented target shells are used to confine the imploding by highpower laser beams. Compared to other fusion ignition schemes,[2–5] the DCI scheme can significantly reduce the energy requirements of the driver laser, improve the robustness of the compression and heating processes, and achieve high energy gain with relatively small laser energy. For the DCI target geometry, the gap between the two compression cones is about 100 μm, the radius of the open cone tips is 50 μm, and the plasma stagnation time is about 300 ps.[6,7] Diagnosing the density distribution of the plasma between the cones with high spatial and temporal resolutions is challenging. This facilitates the understanding of the compression, acceleration, and head-on collision processes in the double-cone ignition scheme.

Typical approaches to investigate the density of the imploding core include neutron activation,[8,9] neutron recoil-reactions,[10,11] the ratio of secondary yields to primary yields,[12] Compton radiography,[13,14] and x-ray radiography.[15–17] The first three methods primarily rely on neutron production through the fusion process to infer the areal density. Consequently, they are suitable for experiments involving high-yield neutron production. X-ray radiography can be used in experiments without or with less neutron production. It can provide a two-dimensional spatial mapping of the areal density, making it a routine diagnostic in fusion experiments. Among the x-ray radiographic schemes, spherically bent crystal imaging[18–20] stands out due to its unique capabilities, including high flux (large acceptance angle), high spatial resolution, and quasi-monochromatic backlight source. Therefore, it has attracted broad interest in high-energy density physics and inertial confinement fusion experiments.

This paper describes in detail the monochromatic crystal backlight imaging (MCBI) system using Cu $K\alpha$ line x-ray emission designed for the Shenguang-II upgrade facility and its application in the DCI experiments. We investigate the backlighter x-ray intensity under various laser conditions and

†Corresponding author. E-mail: zzhang@iphy.ac.cn
‡Corresponding author. E-mail: mhxu@cumtb.edu.cn
§Corresponding author. E-mail: lyj@aphy.iphy.ac.cn

© 2024 Chinese Physical Society and IOP Publishing Ltd

evaluate the spatial resolution of the imaging system, which established the optimal conditions for the backlighting experiments. We report the application of this MCBI system in the DCI experiments, obtaining the areal density, shape, spatial distribution, and uniformity.

2. Design of the MCBI system

Two typical approaches are usually employed to achieve high temporal resolution with MCBI systems. The first is to use a gated x-ray camera, having a time resolution of less than one hundred picoseconds.[21] The second approach is to utilize an ultrashort $K\alpha$ source generated by picosecond-duration laser-foil interactions, giving rise to a time resolution of a few to tens of picoseconds.[22] By controlling the delay time between the compression and backlighter-driver lasers, the time evolution of the plasma can be measured with high temporal resolutions.

Figure 1(a) is the schematic of MCBI with ultrashort x-ray backlighter. The shell material currently employed in the experiments is chlorine-doped plastic ($C_{16}H_{14}Cl_2$) with an initial density of 1.1 g/cm^3–1.2 g/cm^3. The mass-absorption coefficient of $C_{16}H_{14}Cl_2$ is a function of plasma temperature and density. The plasma temperature around the cone tip is below 400 eV at the current Shenguang-II upgrade nanosecond laser capability. Figure 1(b) shows the x-ray transmission as a function of plasma areal density around 10 eV–400 eV for two types of backlighter sources, namely Cu $K\alpha$ (8048 eV) and Ti $K\alpha$ (4511 eV), respectively. Assuming that the measurable transmission of the x-ray backlight system is in the range of 5%–80%[18] (as indicated by the yellow area in Fig. 1(b)), the feasible detection range of plasma areal densities accordingly is 7 mg/cm^2–118 mg/cm^2 for Cu $K\alpha$ backlighter and 1.5 mg/cm^2–23 mg/cm^2 for Ti $K\alpha$ backlighter, respectively. When the areal density of the plasma exceeds 23 mg/cm^2 (for Ti $K\alpha$ backlighter, and 118 mg/cm^2 in the case of Cu $K\alpha$ backlighter), the transmission of the backlighter would be lower than 5%, which in turn leads to inaccurate measurements. Consequently, the backlight system has been designed to utilize the Cu $K\alpha$ backlight to ensure a more accurate diagnostic of high-density plasma generated around the cone tips.

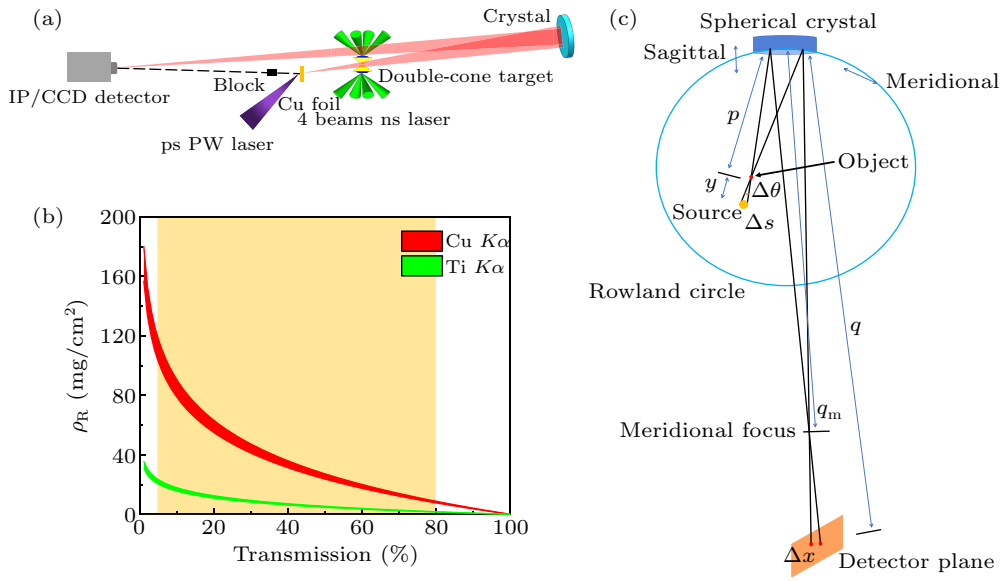


Fig. 1. (a) A schematic of the MCBI system in the experiment. (b) Relationship between backlighter transmission and plasma areal density (ρ_R) around 10 eV–400 eV temperature, where the red area is for Cu $K\alpha$ (8048 eV) and the green area is for Ti $K\alpha$ (4511 eV) and the yellow area is for the x-ray transmission of 5% to 80%. (c) A schematic of the optical path of the spherical crystal imaging systems.

For high spatial resolution imaging, a near-normal incidence between 80° and 90° is commonly employed in MCBI imaging to minimize the aberration. A quartz (2131) crystal was selected as the Bragg crystal to focus the x-ray with an energy of approximately 8048 eV at a Bragg angle of 88.7°. The spherically bent quartz crystal, with a radius of curvature of 400 mm, was positioned 225 mm away from the plasma (or grid), while the detector was located 1804 mm away from the crystal, resulting in a magnification factor of 8.02. To enhance the signal-to-noise ratio, a 3 mm thick tungsten block was used to prevent direct incidence of radiations from the picosecond laser onto the detector. The MCBI system was designed to fit the target chamber of the Shenguang-II upgrade facility,[23] located at the Joint Laboratory of High Power Lasers, Shanghai Institute of Optics and Fine Mechanics, Chinese Academy of Sciences. Through the XOP/Shadow simulations,[24] it had been demonstrated that the crystal can image x-rays within the energy range of 8048 ± 5 eV.

3. Investigation of backlighter intensity and spatial resolution of the MCBI system

To optimize the MCBI system, an experiment was conducted to investigate the impact of different laser parameters

on the intensity of the backlighter x-ray source and the spatial resolution of the system. The experimental setup has been depicted in Fig. 1(a). To generate the x-ray source, an ultraintense picosecond-duration laser beam was employed to irradiate a 20 μm-thick copper foil positioned at 5 mm from the target chamber center (TCC). The four-quadrant gold grid with a bar width of 10 μm and mesh sizes of 60–80–120–160 mesh/cm was positioned at TCC. The x-ray source projected the grid target onto the detector, facilitating the measurement of the spatial resolution of the MCBI system. An Andor iKon-L type charge-coupled device (CCD) and Fujifilm MS type imaging plates (IP)[25,26] were utilized to record the x-ray images. The energy spectrum of the x-ray backlighter was measured using a highly oriented graphite spectrometer (HOPG)[27] with a spectral resolution better than 400, covering an energy range from 7950 eV to 8450 eV. Table 1 displays the parameters of the picosecond laser utilized in the experiment, providing essential details for reference.

Based on the aforementioned laser conditions, the x-ray energy spectra measured with IP detectors are compared in Fig. 2(a). The relationship between backlighter intensity and laser energy is presented in Fig. 2(b). The red triangles in Fig. 2(b) represent the integrated intensity of the images from MCBI, while the black dots indicate the integrated intensity of the backlighter measured by the HOPG spectrometer (Fig. 2(a) within the energy range of 8048 ± 5 eV). It shows a positive correlation between the laser energy and the backlighter intensity.

Table 1. Picosecond laser parameters.

Numbers	Laser energy (J)	Pulse width (ps)	Intensity (10^{18} W/cm^2)
1	19	1.0	2.68
2	96	3.2	4.25
3	286	2.4	9.50
4	444	10.0	6.12

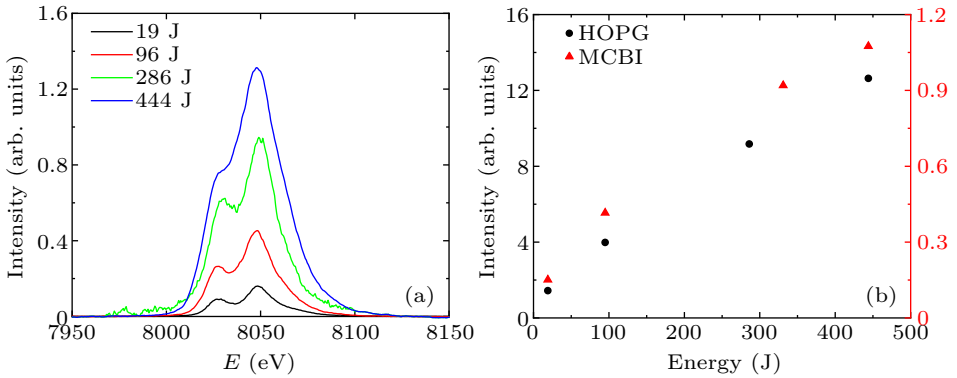


Fig. 2. (a) X-ray energy spectra measured by HOPG spectrometer under different laser energies. (b) The relative intensity of the x-ray backlighter with different laser energies, where the black dots are from HOPG measurements, and the red triangles are from MCBI measurements.

The backlight images on the IP and CCD detectors are presented in Figs. 3(a)–3(d), respectively. Figures 3(a)–3(c) show the results of the grid target imaged on the IP detector under different laser parameters, and Fig. 3(d) shows the results imaged on the CCD detector. The knife-edge spread function of the grid is measured at different positions on the images and subsequently differentiated to obtain the line spread function (LSF). The spatial resolution of the imaging system is determined by defining the full width half maximum (FWHM) of the LSF curve and fitting it with a Gaussian function. Figure 4(a) shows the spatial resolutions of the MCBI system for the x-ray sources of different driving laser intensities, where the black dots are for the IP detector and the red dots are for the CCD detector. The figure clearly demonstrates that the CCD has a better spatial resolution of up to 10 μm in comparison with the IP detector. This difference is mainly attributed to the resolving capability of the two detectors. The pixel size of the CCD detector is 13.5 μm, while for the BAS-MS IP, the actual spatial resolution was measured to be 53 μm[26] when using the Amersham Typhoon^{TM} scanner, even with a 25 μm scan parameter. It means that the CCD detector can provide backlight images with higher quality, which is favorable for the MCBI system. Furthermore, Fig. 4(a) illustrates a gradual decrease in spatial resolution with laser intensity for the IP detector. This phenomenon can be attributed to the increase in the x-ray source size resulting from the lateral transport of fast electrons at higher laser intensities.[28–30] Other researchers have also found that the size of the $K\alpha$ source increases with the laser intensity.[31–33]

The spatial resolution of the backlight system depends on the imaging crystal, the x-ray detectors, and the backlight source, etc. Using the XOP/Shadow program,[24] the spatial resolution determined by the imaging crystal is calculated to be 1.0 μm (assuming the crystal is perfectly manufactured), which only plays a subtle role. By taking into account the magnification of the MCBI system, the resolution of the detector is 6.6 μm for the case of MS IP and 1.7 μm for the case of the CCD camera.

The size of the backlight source also has an influence on the resolution, since different incidence angles will lead

to deviations in the optical path, which in turn result in a decrease in resolution. Here we will derive the spatial resolution according to the imaging optical path as illustrated in Fig. 1(c). Take the meridional direction for example, the deviation Δx in the image plane along this direction satisfies $\Delta x = \Delta s \frac{p}{y} \frac{q-q_{\rm m}}{q_{\rm m}}$, where Δs is the size of the backlight source, p is the object distance, y is the distance between the backlight source and the object, $q_{\rm m} = (Rp\sin\theta)/(2p - R\sin\theta)$ is the focus distance from the crystal in the meridional plane according to the Coddington equation $\frac{1}{p} + \frac{1}{q_{\rm m}} = \frac{2}{R\sin\theta}$, q is the image distance in the experiment optimized by the criteria that the magnification in the meridional plane and in the sagittal plane are equal, that is $(R-p)/(2p-R)$ in the near-normal incidence case, where R is the radius of curvature of the crystal. Dividing Δx by M (the magnification of the imaging system), we can obtain the spatial resolution determined by the source size, $\sigma = \Delta s \frac{p}{y} \frac{(M+1)}{M} (1-\sin\theta) = \Delta\theta p \frac{(M+1)}{M} (1-\sin\theta)$, where θ is the crystal Bragg diffraction angle, and $\Delta\theta = \Delta s/y$ indicates the open angle of the backlight source. The spatial resolution we obtained here from the geometric optical path analysis agrees with those obtained based on spherical aberration analysis,[34,35] both indicating a decrease in resolution with increasing source size. Besides the theoretical calculations, XOP/Shadow simulations are also conducted to investigate the effect of source size on the spatial resolution of the MCBI system. We obtain the spatial resolution of the system with different source sizes when IPs were used as detectors, as shown in Fig. 4(b), where the black dots are simulation results, and the red triangles are experiment measurements. The results indicate that the radius of the $K\alpha$ source is 60 μm–110 μm, assuming the experimental and simulation results are compatible, which is 4–7 times the initial laser focal spot.[36]

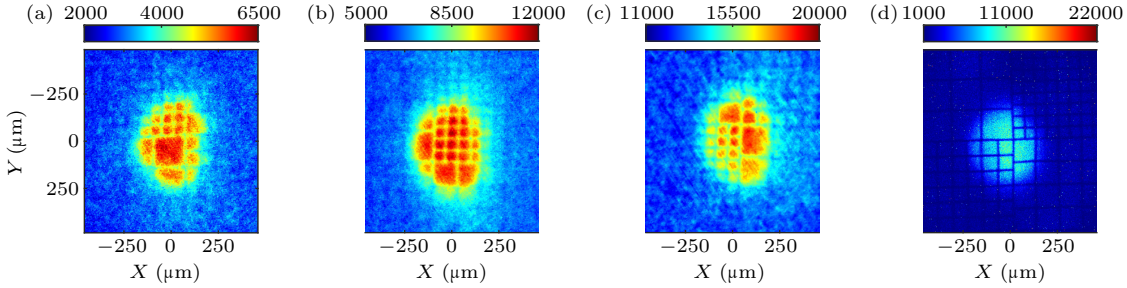


Fig. 3. Backlight images of the grid on the IP/CCD detector. (a) Laser energy 19 J, pulse width 1.0 ps, IP detector. (b) Laser energy 96 J, pulse width 3.2 ps, IP detector. (c) Laser energy 444 J, pulse width 10.0 ps, IP detector. (d) Laser energy 281 J, pulse width 10.0 ps, CCD detector.

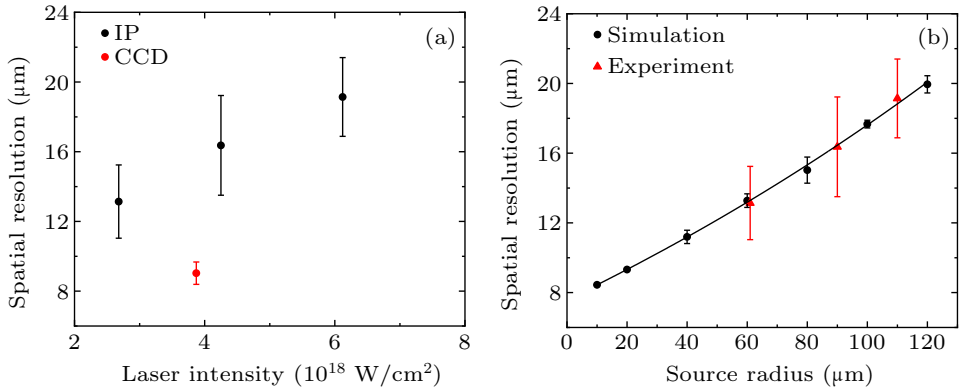


Fig. 4. Spatial resolution of the MCBI system. (a) The spatial resolution with different laser intensities, where the black dots are for the IP detector and the red dots are for the CCD detector. (b) The spatial resolution of the system with different source radii (IPs as detectors), where the black dots are simulation results, and the red triangles are from experimental measurements.

4. Application and experimental results

The developed MCBI system is utilized in the DCI experiments to investigate the spatial distribution and time evolution of the head-on colliding plasma between the cone tips. The nanosecond laser has a wavelength of 0.351 μm and an output energy of 1250 J for each beam. Eight beams are focused and overlapped on the shell, driving the shell compression and acceleration, as shown in Fig. 1(a). The plasma between the cone tips is imaged by Cu $K\alpha$ x-rays generated by the picosecond laser. The evolution of the plasma can be obtained by varying the delay time between the compression laser and the driving laser of the backlighter.

Two-dimensional $K\alpha$ images of the collision plasma are presented in Fig. 5, where the dashed lines mark the shape of a double-cone target and the dashed circle marks the effective region of x-ray imaging. Note that the bright spots at the top and bottom of each figure are due to bremsstrahlung emission of exploding $C_{16}H_{14}Cl_2$ plasma, and the bright spot at the center is the Cu $K\alpha$ backlight image. As shown in Fig. 5(b), at 1.2 ns after the end of the compression laser, the $C_{16}H_{14}Cl_2$ plasma has been accelerated out of the cone tips with a head-on

collision, which formed a clear pattern with reduced intensity at the center due to the absorption of x-rays by the head-on colliding plasma.

Figure 5 compares three x-ray radiographys obtained in similar plasma conditions except probing with different $K\alpha$ sources driven by different picosecond laser parameters. It shows that an image of the highest contrast and quality was achieved with a large driving energy (493 J), leading to a brightest backlight source, and with a relatively low laser intensity, leading to a relatively small source size, as displayed in Fig. 5(b). By analyzing the intensity distribution across the cone wall, we can also conclude that the spatial resolution in the case of Fig. 5(b) is superior to that in Figs. 5(a) and 5(c), since the backlight intensity across the cone wall increases from 10% to 90% over the shortest distance. This conclusion is consistent with that from Fig. 4(a). The spatial distribution of the colliding plasma between the cone tips is clearly demonstrated in this case. With a higher signal-to-noise ratio, it is possible to accurately measure the areal density and provide more precise information about the size and distribution of the plasma. It shows that at the beginning of the head-on colliding process, the plasma still exhibits a symmetrical distribution. The transverse dimension is approximately 150 μm (FWHM).

To further explore the dynamic imaging, an analysis is conducted on the background noise level. As can be seen, with an energy of 493 J and a pulse duration of 10 ps for the backlighter laser, the background noise is significantly lower than in other cases. This can be attributed to the fact that the focused laser intensity has a minimum despite its highest energy, resulting in a reduced high-energy x-ray and gamma-ray background. It demonstrates that the highest spatial resolution and the best contrast ratio were achieved with the picosecond laser having a large energy and a relatively long duration.

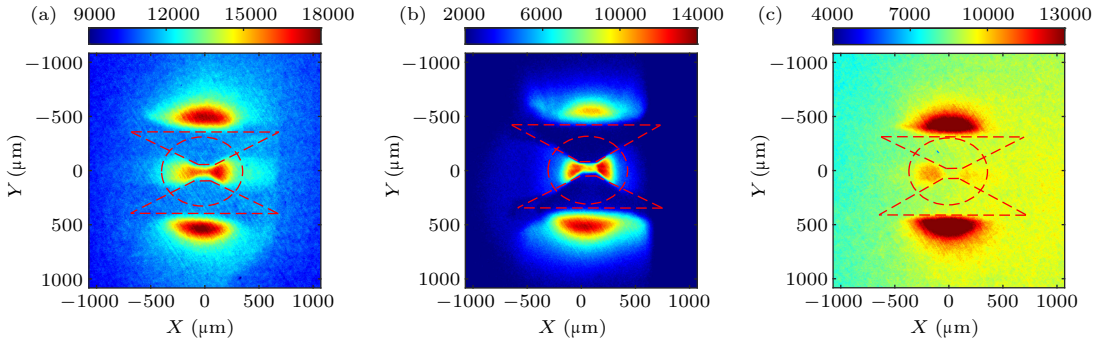


Fig. 5. Two-dimensional $K\alpha$ images of the collision plasma obtained with different $K\alpha$ sources driven by different picosecond lasers at different delay time. (a) Laser energy of 355 J, pulse width of 2.4 ps, and at 1.1 ns after the end of the compression laser. (b) Laser energy of 493 J, pulse width of 10.0 ps, and at 1.2 ns after the end of the compression laser. (c) Laser energy of 94 J, pulse width of 1.0 ps, and at 1.4 ns after the end of the compression laser.

5. Conclusion

We developed a monochromatic crystal backlight imaging system employing spherically bent crystals for the recent double-cone ignition experiments. The system performance was optimized by comparing the results of varying picosecond laser parameters and the recording detectors. The spatial distribution and time evolution of the colliding plasma between the head-on tips were measured with this system. High quality image was obtained with a higher-energy and longer-duration picosecond laser driver. This system would play an important role in understanding colliding plasma dynamics in the DCI scheme.

Acknowledgments

Project supported by the staff of the Shenguang-II upgrade Laser facility. This study was supported by the Strategic Priority Research Program of the Chinese Academy of Sciences (Grant Nos. XDA25010100, XDA25010300, XDA25030100, XDA25030200, and XDA25051000), the National Natural Science Foundation of China (Grant Nos. 11827807 and 12105359), the Open Foundation of Key Laboratory of High Power Laser and Physics of Chinese Academy of Sciences (Grant No. SGKF202105), and the Chinese Academy of Sciences Youth Interdisciplinary Team (Grant No. JCTD-2022-05).

References

[1] Zhang J, Wang W M, Yang X H, *et al.* 2020 *Phil. Trans. R. Soc. A* **378** 20200015
[2] Lindl J D 1994 *AIP Conf. Proc.* **318** 635
[3] Kodama R, Norreys P A, Mima K, *et al.* 2001 *Nature* **412** 798
[4] Azechi H, Sakaiya T, Watari T, *et al.* 2009 *Phys. Rev. Lett.* **102** 235002
[5] Betti R, Zhou C D, Anderson K S, *et al.* 2007 *Phys. Rev. Lett.* **98** 155001
[6] Zhang Z, Yuan X H, Zhang Y H, *et al.* 2022 *Acta Phys. Sin.* **71** 155201 (in Chinese)
[7] Fang K, Zhang Y H, Dong Y F, *et al.* 2023 *Phys. Plasmas* **30** 042705
[8] Abe Y, Nakao A, Arikawa Y, *et al.* 2022 *Rev. Sci. Instrum.* **93** 093523
[9] Mangan M A, Ruiz C L, Cooper G W, *et al.* 2022 *Rev. Sci. Instrum.* **93** 103514
[10] Frenje J A, Casey D T, Li C K, *et al.* 2010 *Phys. Plasmas* **17** 056311
[11] Lahmann B, Johnson M G, Hahn K D, *et al.* 2020 *Rev. Sci. Instrum.* **91** 073501
[12] Johnson M G 2023 *Rev. Sci. Instrum.* **94** 021104
[13] Tommasini R, MacPhee A, Hey D, *et al.* 2008 *Rev. Sci. Instrum.* **79** 10E901

[14] Tommasini R, Hatchett S P, Hey D S, *et al.* 2011 *Phys. Plasmas* **18** 056309

[15] Marshall F J, Mckenty P W, Delettrez J A, *et al.* 2009 *Phys. Rev. Lett.* **102** 185004

[16] Theobald W, Solodov A A, Stoeckl C, *et al.* 2014 *Nat. Commun.* **5** 5785

[17] Fujioka S, Fujiwara T, Tanabe M, *et al.* 2010 *Rev. Sci. Instrum.* **81** 10E529

[18] Sawada H, Daykin T, McLean H S, *et al.* 2017 *Rev. Sci. Instrum.* **88** 063502

[19] Hall G N, Krauland C M, Schollmeier M S, *et al.* 2019 *Rev. Sci. Instrum.* **90** 013702

[20] Kawaguchi C, Flippo K A, Rasmus A M, *et al.* 2021 *Rev. Sci. Instrum.* **92** 093508

[21] Bai X H, Bai Y L, Liu B Y, *et al.* 2011 *Opt. Precis. Eng.* **19** 367

[22] Chen H, Shepherd R, Chung H K, *et al.* 2007 *Phys. Rev. E* **76** 056402

[23] Zhu J Q, Zhu J, Li X C, *et al.* 2018 *High Power Laser Sci. Eng.* **7** e12

[24] Sanchez del Rio M and Dejus R J 2004 *Proc. SPIE* **5536** 171

[25] Miyahara J, Takahashi T, Amemiya Y, *et al.* 1986 *Nucl. Instrum. Methods Phys. Res. Sect. A* **246** 572

[26] Dong Y F, Zhang Z, Xu M H, *et al.* 2020 *Rev. Sci. Instrum.* **91** 033105

[27] Sakata S, Lee S, Morita H, *et al.* 2018 *Nat. Commun.* **9** 3937

[28] Reich C H, Uschmann I, Ewald F, *et al.* 2003 *Phys. Rev. E* **68** 056408

[29] Li Y T, Yuan X H, Xu M H, *et al.* 2006 *Phys. Rev. Lett.* **96** 165003

[30] Lin X X, Li Y T, Liu B C, *et al.* 2010 *Phys. Rev. E* **82** 046401

[31] Rousse A, Audebert P, Geindre J P, *et al.* 1994 *Phys. Rev. E* **50** 2200

[32] Wharton K B, Hatchett S P, Wilks S C, *et al.* 1998 *Phys. Rev. Lett.* **81** 822

[33] Feurer T, Forster E, Gibbon P, *et al.* 1999 *Applications of High Field and Short Wavelength Sources VIII*, 1999, Washington D.C., pp. 108–110

[34] Schollmeier M S, Geissel M, Shores J E, *et al.* 2015 *Appl. Opt.* **54** 5147

[35] Harding E C, Robertson G K, Dunham G S, *et al.* 2023 *Rev. Sci. Instrum.* **94** 083509

[36] Stephens R B, Snavely R A, Aglitskiy A, *et al.* 2004 *Phys. Rev. E* **69** 66414